Supporting Information

Synthesis of a New Series of Anthraquinone-Linked Cyclopentanone Derivatives: Investigating the Antioxidant, Antibacterial, Cytotoxic, Tyrosinase Inhibitory Activities of the Mushroom Tyrosinase Enzyme Using Molecular Docking

Experimental Section

2,6,11-Trioxo-3-phenyl-*N*-(*p*-tolyl)-2,3,6,11-tetrahydro-1*H*-cyclopenta[*a*]anthracene-1-carboxamide (2)

Yield 79%; mp 156°C; IR (cm^{-1}): 2765 (Ar-NH), 3274 (NH), 1733 (C=O); ^{1}H NMR (300MHz, DMSO-d_6): 8.29-7.88 (4H, d, Ar); 7.57-7.40 (d, 2H, Ar); 7.56-7.21 (Ar, 4H, d); 7.23-6.77 (m, ph, 5H); 7.23 (s, -NH, 1H); 4.92 (s, $-CH_2$, 2H); 4.58 (s,$-CH_2$, 2H); 4.0 (1H, CH-NH-ph, s); ^{13}C NMR (75 MHz, DMSO-d_6): 206.0 (1C, -C=O); 185.2-182.1 (2C, C=O); 147.2-128.9 (6C, Ar ring); 168.2 (1C, C=O); 147.2-128.9 (6C, Ar ring); 136.2-125.0 (6C, C=O); 133.6-126.8 (6C, Ar ring); 58.9 (1C, C=O); 58.4 (1C, -CH); 21.3 ($-CH_3$, 1C); EI-MS (*m/z*): 472.15(M^+, 33.9%); Elemental analysis: CalcdFor (C_{31} $H_{21}NO_4$): C, 78.97; H, 4.49; N, 2.97% Found: C, 78.91; H, 4.48; N, 2.93%.

***N*-(4-Methoxyphenyl)-2,6,11-trioxo-3-phenyl-2,3,6,11-tetrahydro-*1H*-cyclopenta[*a*]anthracene-1-carboxamide (3)**

Yield 82%; mp 159°C; IR (cm^{-1}): 2683 (Ar-NH), 3168 (NH), 1713 (C=O); ^{1}H NMR (300 MHz, DMSO-d_6): 8.29-7.88 (Ar, 4H, d); 7.57-7.38 (2H, d, Ar); 7.49-6.97 (Ar, 4H, d); 7.24-6.77 (m, Ar, 5H); 7.23 (1H, s, C=O); 4.92 (s, $-CH_2$, 2H); 4.58 (s,$-CH_2$, 2H);4.0 (s, NH-ph, 1H); 3.83 (s, -O-, 3H); ^{13}C NMR (75 MHz, DMSO-d_6): 206.0 (1C, -C=O); 185.2-182.1 (2C, C=O); 158.9-114.5 (6C, C=O); 147.2-128.9 (6C, Ar ring); 168.2 (1C, C=O); 147.2-128.9 (6C, Ar ring); 133.6-126.8 (6C, Ar ring); 58.9 (1C, C=O); 58.4 (1C, -CH); 55.8 ($-CH_3$, 1C); EI-MS (*m/z*): 488.15 (M^+, 34.0%); Elemental analysis: Calcd. For (C_{31} $H_{21}NO_5$): C, 76.38; H, 4.34; N, 2.87% Found: C, 76.34; H, 4.37; N, 2.85%.

***N*-(4-Bromophenyl)-2,6,11-trioxo-3-phenyl-2,3,6,11-tetrahydro-1*H*-cyclopenta[*a*]anthracene-1-carboxamide (4)**

Yield 89%; mp 151°C; IR(cm^{-1}): 2676 (Ar-NH), 3264 (NH), 1697 (C=O); ^{1}H NMR (300MHz, DMSO-d_6): 8.29-7.88 (d, 4H, Ar): 7.70-7.58 (d, 4H, Ar); 7.23-6.77 (d, 5H, Ar); 7.57-7.40 (Ar, d, 2H); 7.23 (s, -NH, 1H); 4.92 (s, $-CH_2$, 2H); 4.58 (s,$-CH_2$, 2H); ^{13}C NMR (75 MHz, DMSO-d_6): 206.0 (1C, -C=O); 185.2-182.1 (2C, C=O); 137.6-121.9 (6C, C=O); 147.2-128.9 (6C, Ar ring); 168.2 (1C, C=O); 147.2-128.9 (6C, Ar ring); 133.6-126.8 (6C, Ar ring); 58.9 (1C, C=O); 58.4 (1C, -CH); EI-MS (*m/z*): 537.04 (M^+, 97.4%); Elemental

analysis: Calcd For ($C_{3O}H_{18}BrNO_4$): C, 67.18; H, 3.38; N, 2.61% Found: C, 67.16; H, 3.39; N, 2.65%.

_N_-(2-chlorophenyl)-2,6,11-trioxo-3-phenyl-2,3,6,11-tetrahydro-1_H_-cyclopenta[_a_]anthracene-1-carboxamide (5)

Yield 72%; mp 140°C; IR (cm^{-1}): 2732 (Ar-NH), 3194 (NH), 1724 (C=O); ^{1}H NMR (300MHz, DMSO-d_6): 8.04-7.13 (d, ph, 4H); 7.66-7.17 (d, Ar, 4H); 7.23 (s, ph-NH-C=, 1H); 7.23-6.77 (m, 5H, ph); 7.18-7.02 (CH-CH, d, 2H); 4.92 (2H, s, -CH_2); 4.58 (-CH_2, s, 2H);^{13}C NMR (75 MHz, DMSO-d_6): 206.0 (1C, -C=O); 185.2-182.1 (2C, C=O); 147.2-128.9 (6C, Ar ring); 168.2 (1C, C=O); 147.2-128.9 (6C, Ar ring); 136.2-125.0 (6C, C=O); 133.6-126.8 (6C, Arring); 58.9 (1C, C=O); 58.4 (-CH, 1C); EI-MS (*m/z*): 492.10(M^+, 32.8%); Elemental analysis: CalcdFor ($C_{30}H_{18}ClNO_4$): C, 73.25; H, 3.69; N, 2.85% Found: C, 73.21; H, 3.72; N, 2.87%.

_N_-(4-chlorophenyl)-2,6,11-trioxo-3-phenyl-2,3,6,11-tetrahydro-1_H_-cyclopenta[_a_]anthracene-1-carboxamide (6)

Yield 69%; mp 121°C; IR (cm^{-1}): 2717 (Ar-NH), 3254 (NH), 1685 (C=O); ^{1}H NMR (300MHz, DMSO-d_6): 7.88-8.29 (Ar, d, 4H); 7.58-7.40 (d, 2H, Ar); 7.47-7.75 (d, ph, 4H); 7.26-7.23 (ph, m, 5H); 7.23 (s, -NH, 1H); 4.92 (s, -CH_2, 2H); 4.58 (s,-CH_2, 2H); ^{13}C NMR (75 MHz, DMSO-d_6): 206.0 (1C, -C=O); 185.2-182.1 (2C, C=O); 147.2-128.9 (6C, Ar ring); 168.2 (1C, C=O); 147.2-128.9 (6C, Ar ring); 136.2-120.4 (6C, C=O); 132.4-126.2 (6C, Arring); 58.9 (1C, C=O); 58.4 (-CH, 1C); EI-MS (*m/z*): 492.10(M^+, 32.8%); Elemental analysis: CalcdFor ($C_{30}H_{18}ClNO_4$)C, 73.25; H, 3.69; N, 2.85% Found: C, 73.21; H, 3.72; N, 2.87%.

_N_-benzyl-2,6,11-trioxo-3-phenyl-2,3,6,11-tetrahydro-1_H_-cyclopenta[_a_]anthracene-1-carboxamide (7)

Yield 77%; mp 132°C; IR (cm^{-1}): 2687 (Ar-NH), 3189 (NH),1728 (C=O); ^{1}H NMR (300MHz, DMSO-d_6): 8.29-7.88 (Ar, d, 4H): 8.03 (s, -NH, 1H); 757-7.40 (Ar, 2H, d); 7.33-7.23 (10H, m, ph); 4.92 (s, -CH_2, 2H); 4.58 (s, 2H, -CH_2); 4.40 (s, -CH_2, 2H):^{13}C NMR (75 MHz, DMSO-d_6): 206.0 (1C, -C=O); 185.2-182.1 (2C, C=O); 147.2-128.9 (6C, Ar ring); 168.2 (1C, C=O); 147.2-128.9 (6C, Ar ring); 136.2-125.0 (6C, C=O); 133.6-126.8 (6C, Ar ring); 58.9 (1C, C=O); 58.4 (1C, -CH); 43.6 (-CH_2, 1C)EI-MS (*m/z*): 472.15 (M^+, 33.9%);

Elemental analysis: CalcdFor ($C_{31}H_{21}NO_4$): C, 78.97; H, 4.49; N, 2.97% Found: C, 78.99; H, 4.51; N, 2.92%.

2,6,11-trioxo-*N*,3-diphenyl-2,3,6,11-tetrahydro-1*H*-cyclopenta[*a*]anthracene-1-carboxamide (8)

Yield 72%; mp 159°C; IR (cm^{-1}): 2728 (Ar-NH), 3283 (NH), 1736 (C=O); ^1H NMR (300MHz, DMSO-d_6): 8.29, 7.86 (d, Ar, 4H); 7.54-7.40 (d, Ar, 2H); 7.61-7.19, (m, ph, 5H); 7.33-7.23 (m, ph, 5H); 4.92 (s, -CH_2, 2H); 4.56 (s,-CH_2, 2H); 4.0 (s, CH-NH-ph, 1H); ^{13}C NMR (75 MHz, DMSO-d_6): 206.0 (1C, -C=O); 185.2-182.1 (2C, C=O); 147.2-128.9 (6C, Ar ring); 168.2 (1C, C=O); 147.2-128.9 (6C, Ar ring); 132.4-126.2 (6C, C=O); 133.6-126.8 (6C, Ar ring); 58.9 (1C, C=O); 58.4 (1C, -CH);EI-MS (*m/z*): 458.13 (M^+, 32.8%); Elemental analysis: CalcdFor ($C_{30}H_{19}NO_4$): C, 78.76; H, 4.19; N, 53.06% Found C, 78.80; H, 4.21; N, 53.01%.

Cytotoxicity activity

The cytotoxicity activity of synthesised compounds (**1-8**) were evaluated aganist MCF-7 cell line and normal Vero cell line, and all of them showed low activity compared to other standard doxorubicin (LC_{50}: 0.74± 0. 01 µg/mL) shown in Table 4 Three cell lines were treated with these compounds at one primary cytotoxic assay dose of 100µM for 48 h (MTT anticancer assay). Doxorubicin was used as a standard.

The current protocol involved pre-incubating all cell lines on a microtitre plate and measuring the growth percentage of treated cells compared to untreated control cells. Compounds were considered to have cytotoxic activity if they reduced the growth of any cell line by approximately 32% or less. A 0.1mL aliquot of the cell suspension (containing 5 × 10^6 cells per 100 µL) and 0.1 mL of the test solution (ranging from 6.25 to 100 µg in 1% DMSO, with a final DMSO concentration in the media below 1%) were added to the wells, and the plates were incubated in an incubator with 5% CO_2 at 37 °C for 72 h. The blank sample contained only the cell suspension, whereas the control wells contained 1% DMSO and the cell suspension. After 72 h, 20 µL of MTT was added, followed by the addition of propanol (100 µL) after a 2 h incubation in the CO_2 incubator. The plates were then protected from light with aluminum foil and agitated in a rotary shaker for 10-20 minutes. Finally, the absorption data at 562 nm were obtained using an ELISA reader.

Inhibitory mechanism

The activities of compounds 1 and 2 were examined in relation to the oxidation of L-dihydroxyphenylalanine (L-DOPA) by mushroom tyrosinase at various concentrations. The initial reaction rates were determined by monitoring dopachrome formation at 475 nm. As shown in Figure 5, the Lineweaver-Burk plots of 1/V versus 1/[S] resulted in a family of straight lines with the same vertical intercept. In this figure, the abscissa 1/[L-DOPA] is the reciprocal of the L-dihydroxyphenylalanine (L-DOPA) concentration, whereas the ordinate 1/V is the reciprocal of the reaction rate, reflecting the reciprocal of tyrosinase activity. The plots indicated that compound 2 (Ki = 11.2 mM at 25 mM) is a competitive inhibitor, and its inhibitory activity decreases with increasing substrate concentration. In contrast, the low-activity compound 1 exhibited noncompetitive behaviour.[1]

Docking

In comparison to kojic acid, which has a binding affinity of -4.7 kcal/mol, compound 2 has a binding affinity of (-1.6 kcal/mol). As kojic acid is a commonly used insecticide to kill mosquitoes, it was used as a benchmark. The stability of protein-ligand interactions is greatly influenced by the hydrogen bond, which is formed when two atoms are located at a favourable distance of less than 3.5 Å. The compounds (1–8) having strong hydrogen bonds to the corresponding 2Y9X proteins had bond lengths less than 3.5 Å; Compound 2 forms hydrogen bonds with the receptor 2Y9X, as shown in Figure 5. Hydrogen-interacting amino acid residues with a bond length of 2.53 Å are referred to as Asp 438. Pro 189, Lys 190, Ile 191, Pro 334, Val 404, Glu 405, Arg 406, Ser 407, Ala 413, Tyr 415, Lys 435, Pro 436, Leu 437, Asp 438, Pro 439, and Thr 440 are among the residues of amino acids that make up the protein 2Y9X. The Asn 323, and Asn 332, of kojic acid, having a bond length of 1.70 to 1.78 Å, respectively are interfering residues interacting with hydrogen. Thr 321, Asn 323, Gly 331, Asn 332, Thr 333, Pro 334, Val 404, Glu 405, Ser 407, Ser 412, Ala 413, Tyr 415, Asp 438, and Pro 436 are among the amino acid residues shown in Figure 6.

Molecular dynamics simulations

Molecular dynamics simulation was carried out using Desmond and Schrödinger software to explore the stability of ligand (compound **2)** docked complexes with

proteins 2Y9X. The ligand topology was generated by the PRODRG server and combined with the protein topology using the GROMOS 43a1 force field and a solvation method involving a single point charge (SPC) water model. The system was framed with a cubic box at a distance of 2 nm from the box to the protein surface. The necessary ions were added to neutralise the system, and the docked complex energy was minimised using the steepest descent algorithm. The LINCS algorithm was used to constrain the bond lengths and electrostatics computed using the PME method. The NVT and NPT ensembles were used to equilibrate the systems for each 100 ps, with a reference temperature of 300 K, using the V-rescale thermostat. The production MD run was conducted for 10 ns with a time step of 2 fs, and the docked complex structure coordinates were saved every 10 ps for further analysis. The results were analysed using RMSD, RMSF, gyration, and hydrogen bond plots, and Xmgrace software was used to plot the graphs.

RMSD analysis

The Root Mean Square Deviation (RMSD) values were used to assess the stability of the complex structures. Upon analysing the RMSD plot of complex 2Y9X in relation to compound 2, it was determined that the complex exhibited stability between 20 and 40 ns. This was evident from the peak fluctuation of the Cα backbone of the protein and heavy atoms of the ligand, which were found to be within the range depicted in Figure 7 and provided valuable insights into their stability.

RMSF analysis

RMSF analysis was performed to assess changes in the protein chain during the simulation. No fluctuations were detected in the amino acid residues, except for the N- and C-terminal residues, which were within an unacceptable range (Figure 8). According to the MD simulation analysis, compound 2 displayed stability and showed favourable interactions with crucial protein residues (Figures 7-10). Consequently, these compounds may prove to be effective inhibitors of 2Y9X proteins.

Structure-activity relationships

The presence of both hydrophilic and hydrophobic moieties in anthracene-9,10-dione is crucial for its antibacterial activity. Hydrophobic substituents, such as prenyl groups,

alkylamino chains, alkyl chains, and nitrogen- or oxygen-containing heterocyclic moieties, are essential in this compound.[2]As shown in Figure 10, compound 2, which has para -CH_3 (methyl group enhances lipophilicity) with 6-phenyl-hexane-2,4-dione connected hydrazinyl,has low antibacterial activity, and compound 2 (13.45±0.24 µg/mL) is formed from 1,4-dihydroxyanthracene-9,10-dione, benzaldehyde, and a compound containing 3-oxo-N-(o-tolyl) butanamide group. It demonstrated higher tyrosinase inhibition activities and it has (39.08 µg/mL) higher antioxidant activity (100 µg/mL) than others; also, it showed antibacterial activity only against S. aureus (10 µg/mL); Compound 2 has moderate activity against both S. aureus (10 µg/mL) and E. coli (8 µg/mL), as indicated in Figure 4.

The antibacterial properties of the compound were improved by its lipophilicity; however, as the molecular weight of the compound increased, its antimicrobial properties decreased.[3] The ability of log (Ko/w) to integrate into the cell wall and membrane, as measured by its lipophilicity, may be impeded by the steric effects of the compound, as suggested by its molecular weight.[4] Our discovery stimulated us to delve deeper into investigating additional derivatives featuring this core structure equipped with various substituents, with the intention of gaining a more comprehensive grasp of the structure-activity relationship (SAR) of this scaffold. The conclusion drawn was that the anthraquinone group might be situated in the outer part of the active pocket, similar to anthracene-9,10-dione, which exhibited greater tolerance towards the structure of ligands. This hypothesis was subsequently verified using molecular simulations. Moreover, the anthraquinone moiety occupied a subpocket formed by Asp 438 outside the cavity and an H-bond interaction between the carbonyl of anthraquinone and the amino acid Asp 438. PRO 189, LYS 190, ILE 191, PRO 334, VAL 404, GLU 405, ARG 406, SER 407, ALA 413, TYR 415, LYS 435, PRO 436, LEU 437, ASP 438, PRO 439, and THR 440 were observed. The SAR results obtained in this study can be reasonably explained by the observed interactions. In order to gain insight into the structure-activity relationship (SAR) of compound (1-8), we performed numerous structural modifications and synthesised a series of new analogues as part of our ongoing study of Anthraquinone-Linked Cyclopentanone Derivatives.

^{1}H and ^{13}C NMR spectrum of Compound (1a-1i)

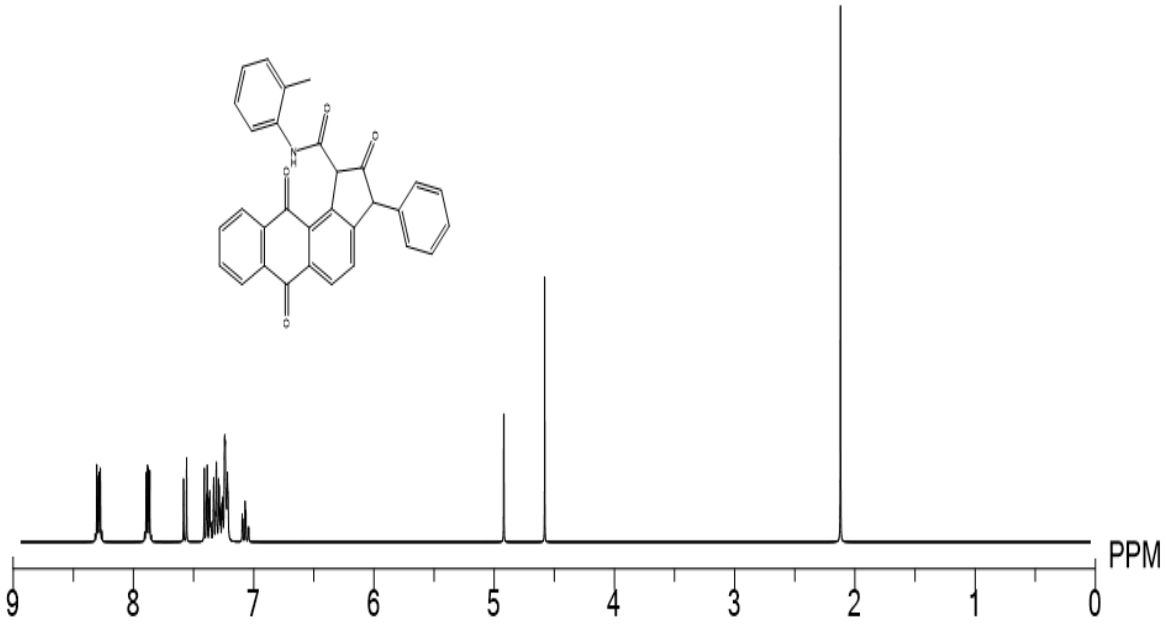

Figure S1. ^{1}H NMR spectrum of the compound **1**

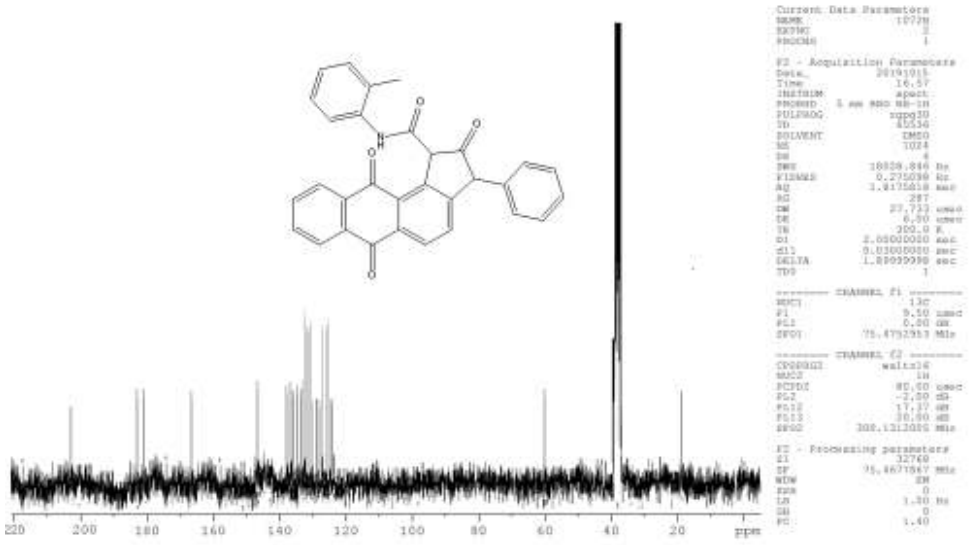

Figure S2. ^{13}C NMR spectrum of the compound **1**

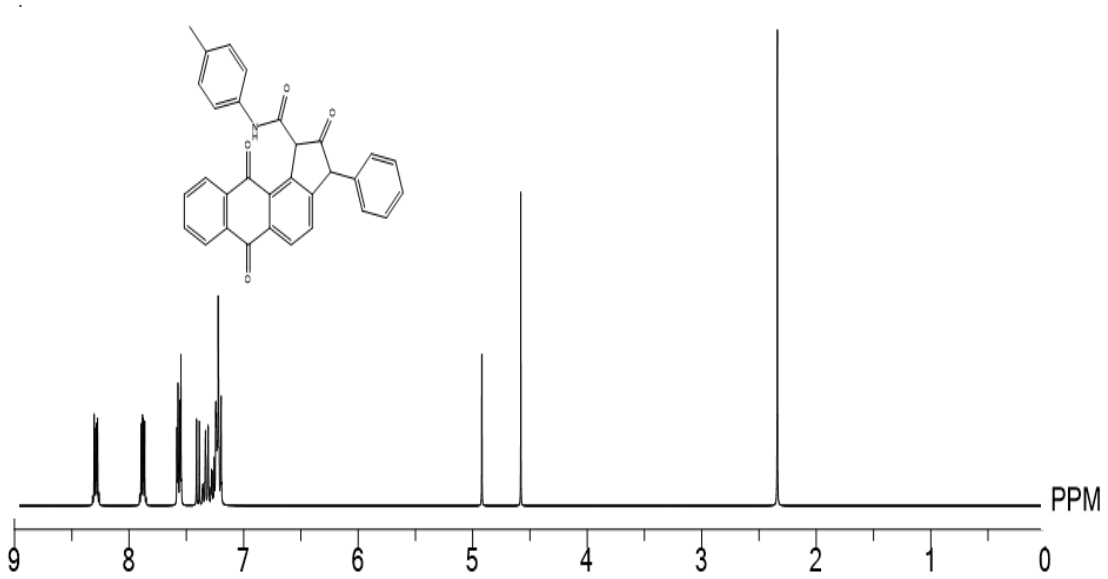

Figure S3. ^{1}H NMR spectrum of the compound **2**

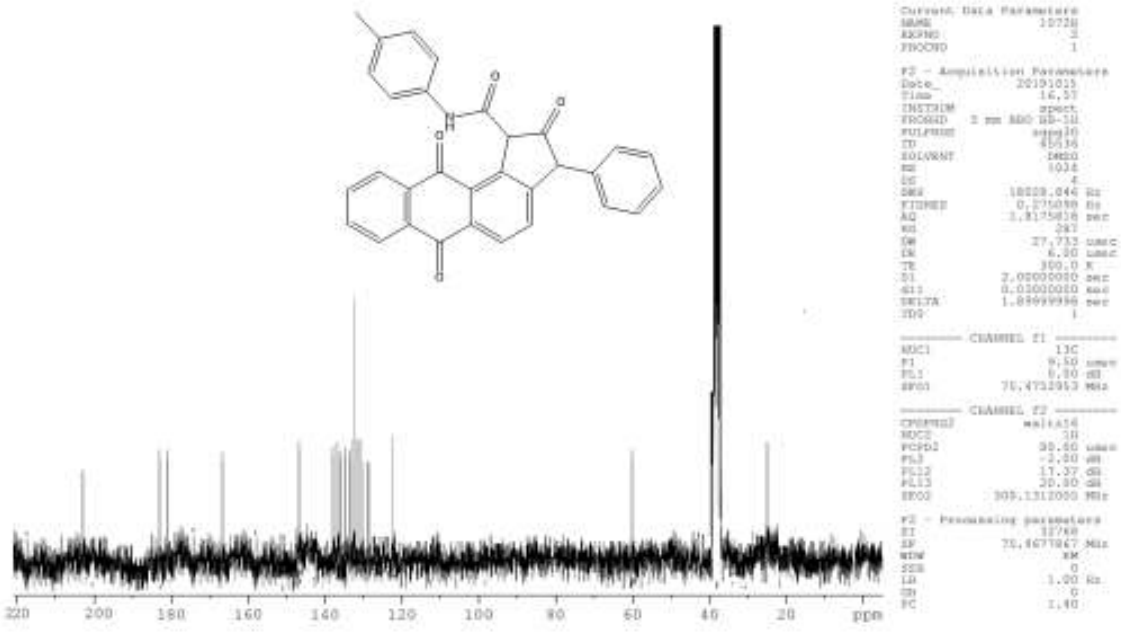

Figure S4. ^{1}H NMR spectrum of the compound **2**

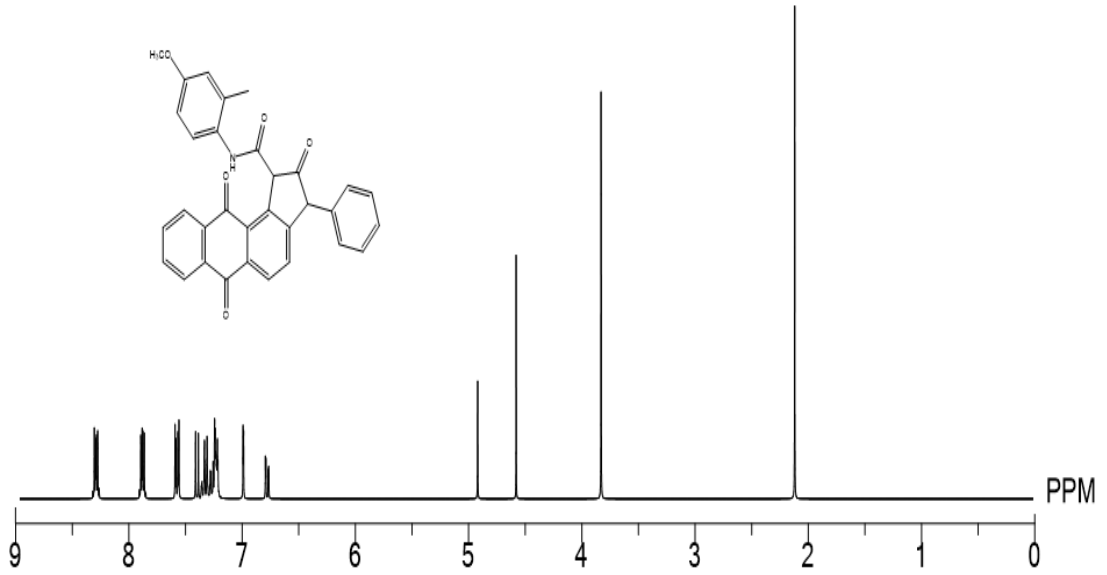

Figure S5. ^{1}H NMR spectrum of the compound **3**

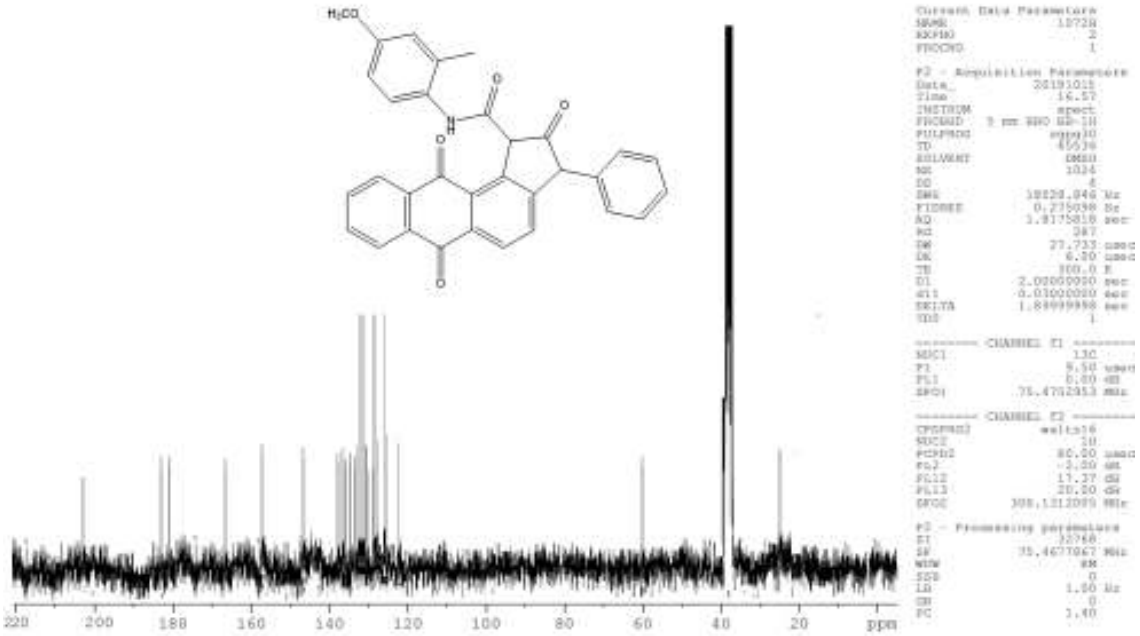

Figure S6. ^{1}H NMR spectrum of the compound **3**

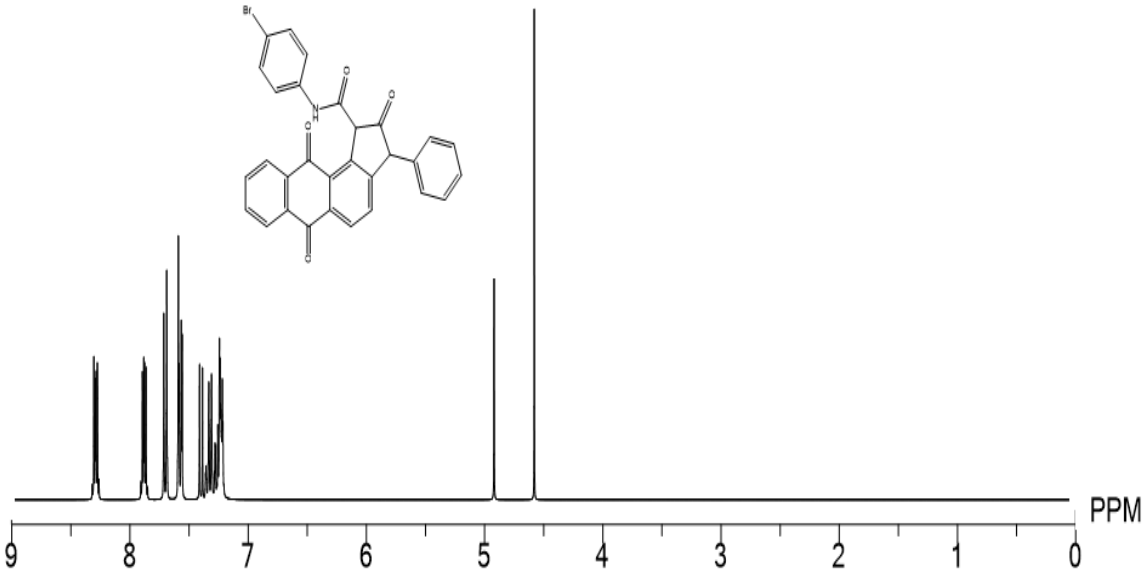

Figure S7. ^{1}H NMR spectrum of the compound **4**

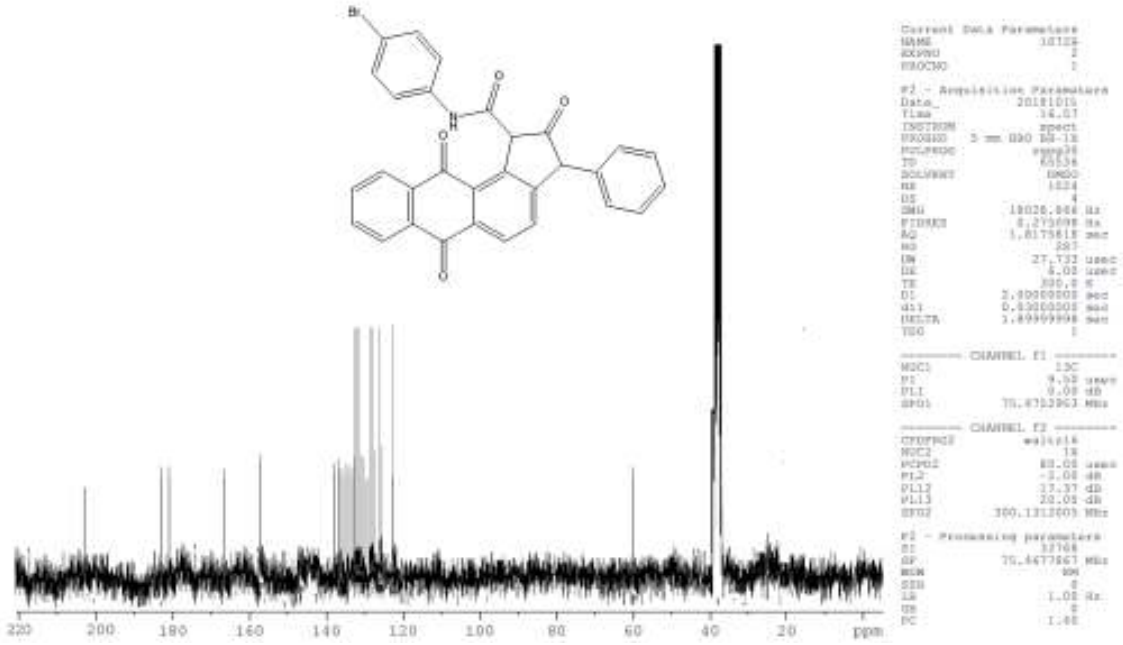

Figure S8. ^{1}H NMR spectrum of the compound **4**

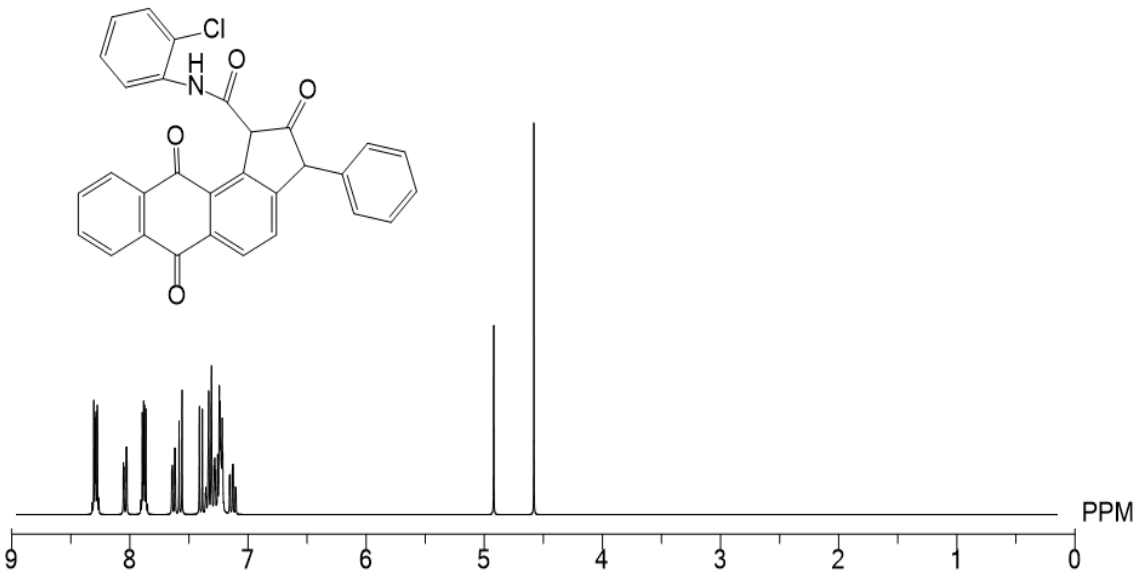

Figure S9. ^{1}H NMR spectrum of the compound **5**

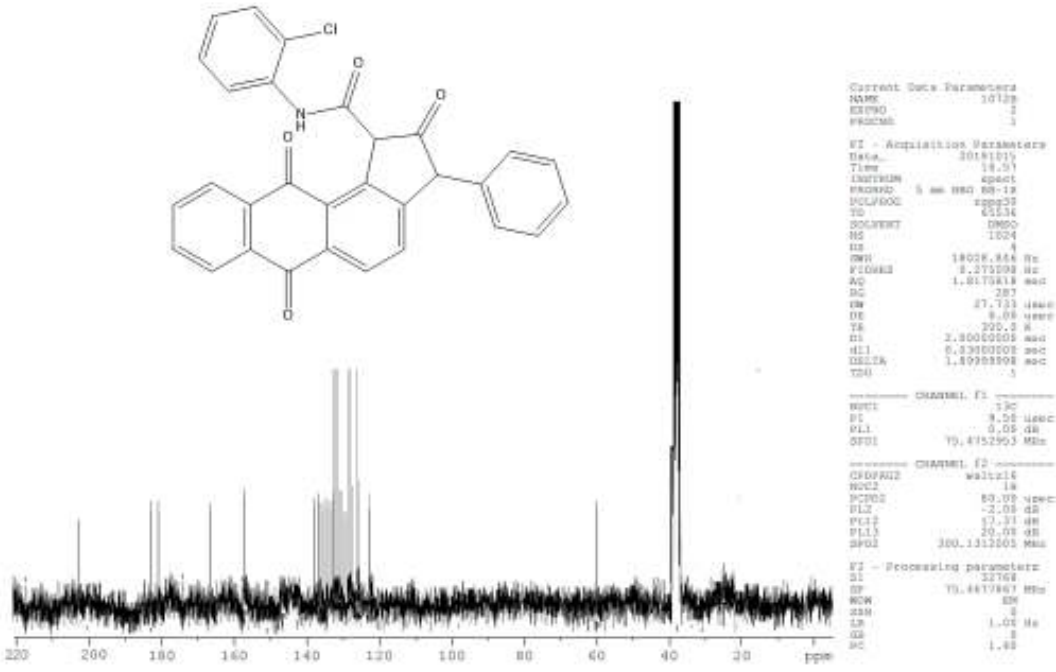

Figure S10. ^{1}H NMR spectrum of the compound **5**

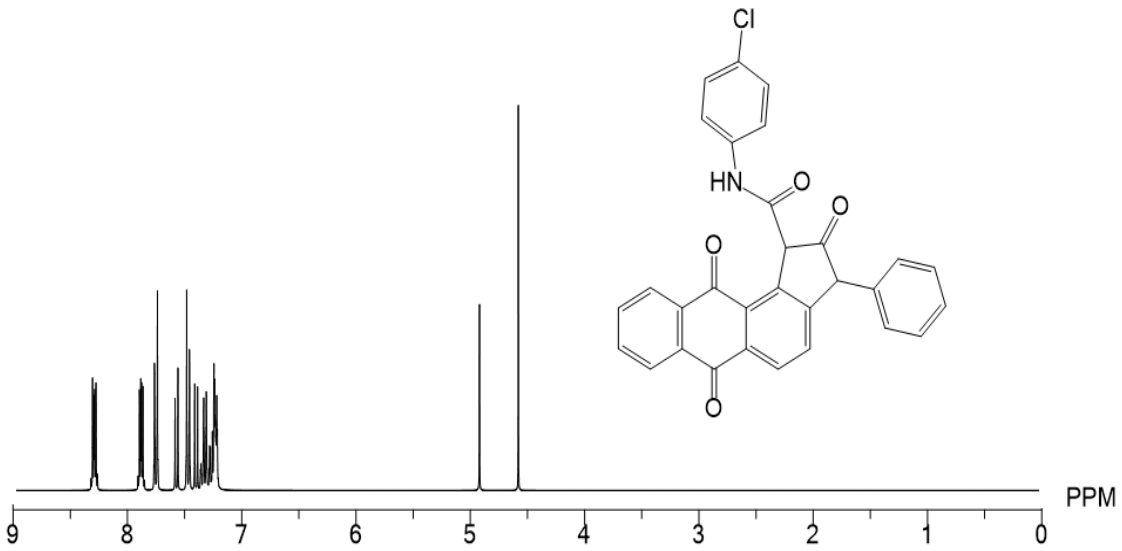

Figure S11. ^{1}H NMR spectrum of the compound **6**

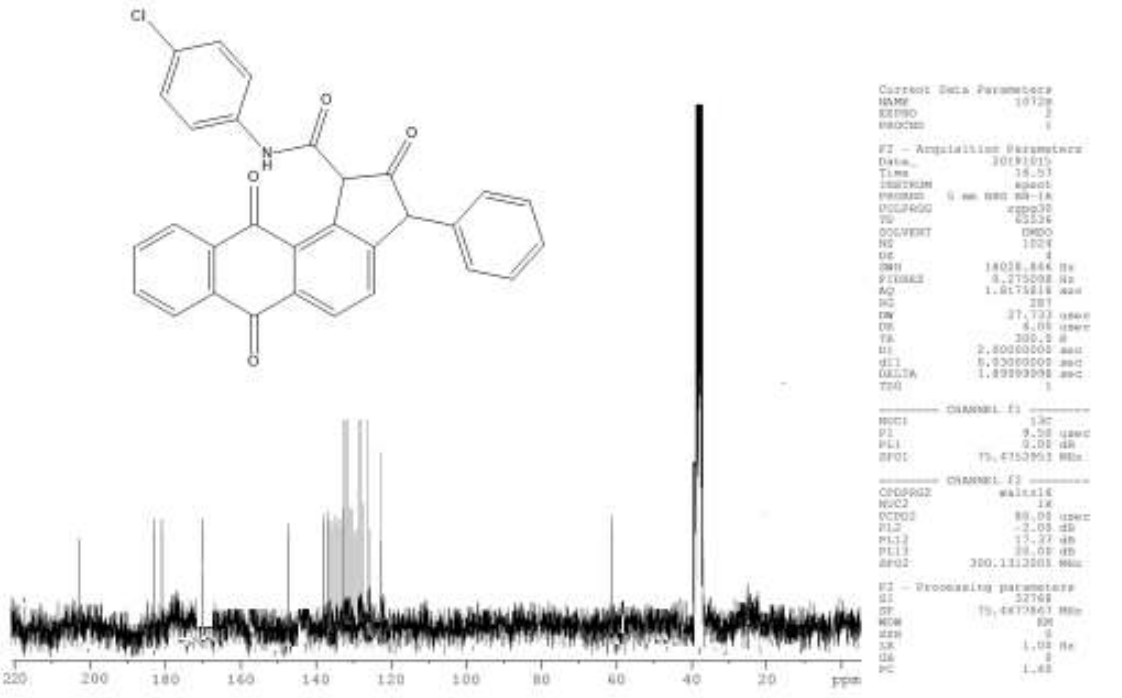

Figure S12. ^{1}H NMR spectrum of the compound **6**

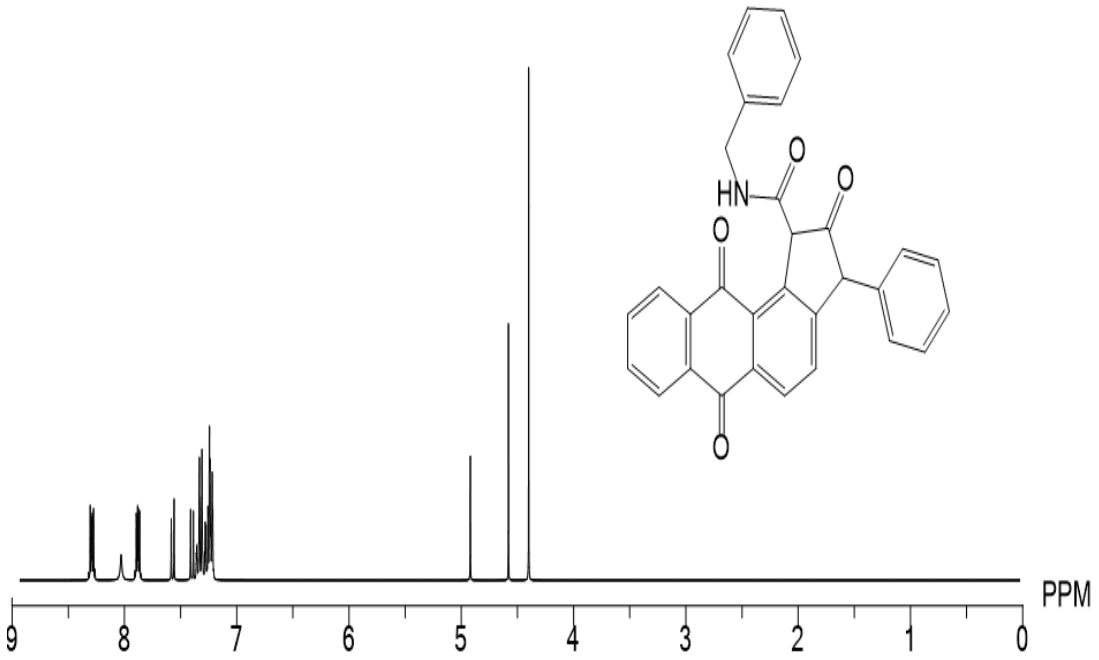

Figure S13. ^{1}H NMR spectrum of the compound **7**

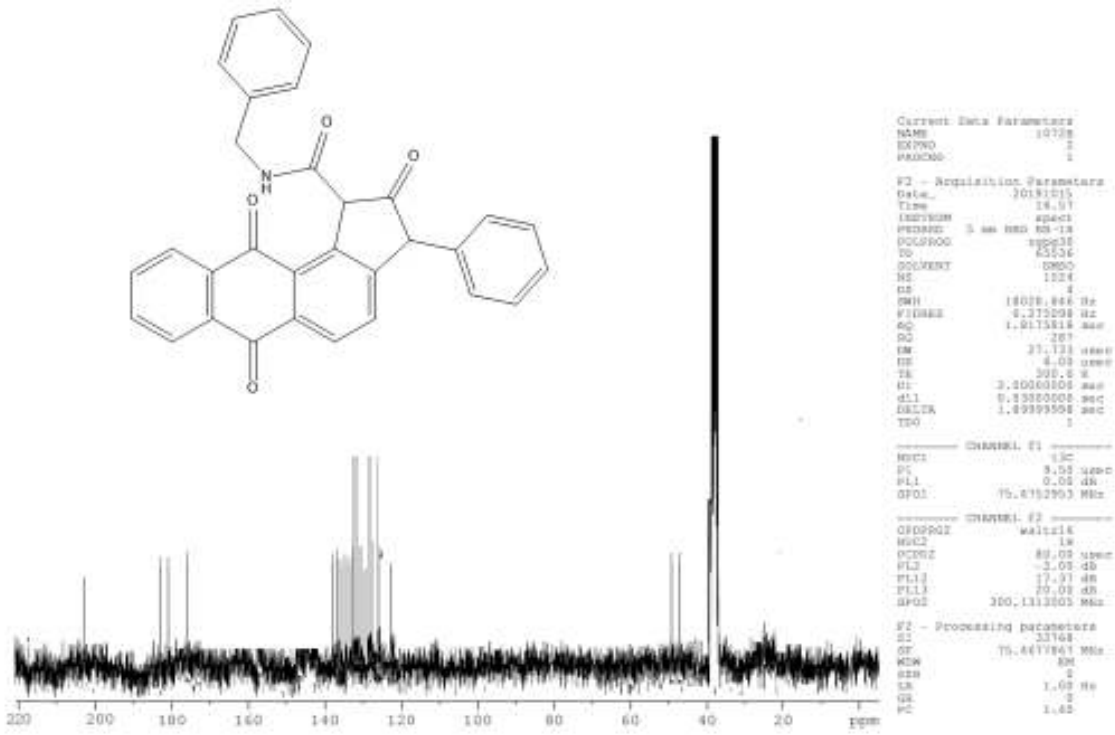

Figure S14. ^{1}H NMR spectrum of the compound **7**

Figure S15 ^{1}H NMR spectrum of the compound **8**

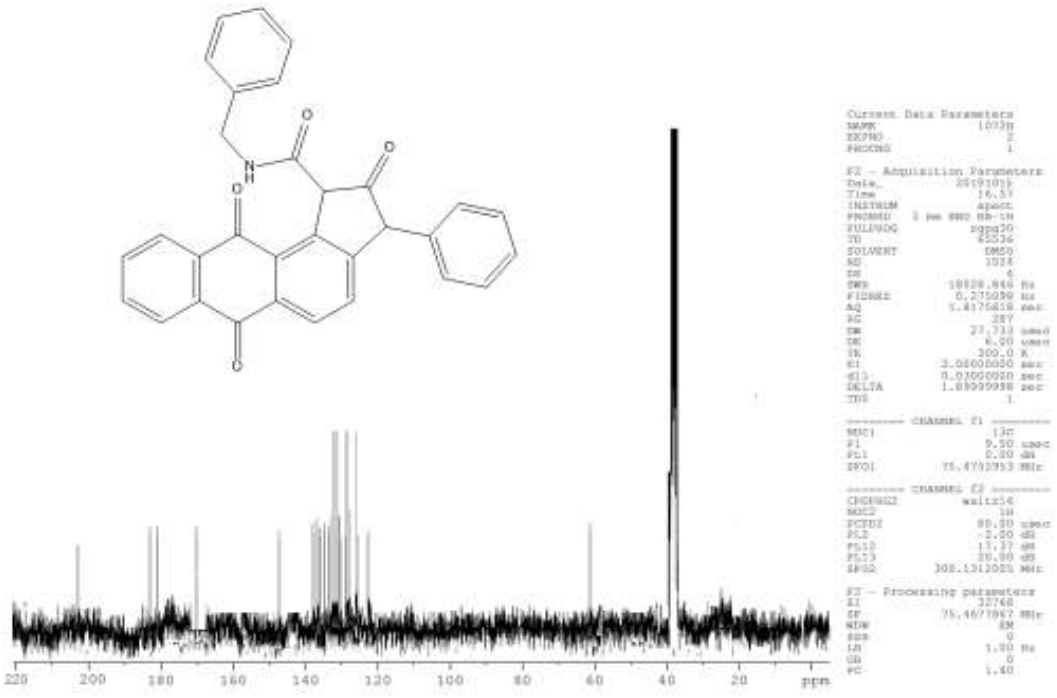

Figure S16. ^{1}H NMR spectrum of the compound **8**

Reference

1. G. Battaini, E. Monzani, L. Casella, L. Santagostini, R. Pagliarin, J. Biol. Inorg. Chem. 5 (2000) 262e268.
2. Fotie, J., Matherne, C.M., Mather, J.B., Wroblewski, J.E., Johnson, K., Boudreaux, L.G. and Perez, A.A., 2023. The Fundamental Role of Oxime and Oxime Ether Moieties in Improving the Physicochemical and Anticancer Properties of Structurally Diverse Scaffolds. International Journal of Molecular Sciences, 24(23), p.16854. https://doi.org/10.3390/ijms242316854
3. Houshmand, A., Heroux, D., Liu, D.Y., Zhou, W., Linington, R.G., Bally, M., Warren, J.J. and Walsby, C.J., 2022. Ferrocene-appended anthraquinone and coumarin as redox-active cytotoxins. Dalton Transactions, 51(30), pp.11437-11447. https://doi.org/10.1039/D2DT01251K
4. Lian, G., Chen, T., Kattou, P., Yang, S., Li, L. and Han, L., 2021. Understanding drug delivery outcomes: Progress in microscopic modeling of skin barrier property, permeation pathway, Dermatopharmacokinetics, and bioavailability. Fundamentals of Drug Delivery, pp.171-191. https://doi.org/10.1002/9781119769644.ch7